In-Vivo Synthetic Aperture and Plane Wave High Frame Rate Cardiac Imaging

Stuart, Matthias Bo; Jensen, Jonas; Brandt, Andreas Hjelm; Nikolov, Svetoslav; Nielsen, Michael Bachman; Jensen, Jørgen Arendt

Published in:
Proceedings of IEEE International Ultrasonics Symposium

Link to article, DOI:
10.1109/ULTSYM.2014.0298

Publication date:
2014

Document Version
Early version, also known as pre-print

Paper presented at the IEEE International Ultrasonics Symposium, Chicago, Il., USA, 2014:

In-Vivo Synthetic Aperture and Plane Wave High Frame Rate Cardiac Imaging

Matthias Bo Stuart, Jonas Jensen, Andreas Hjelm Brandt, Svetoslav Ivanov Nikolov, Michael Bachmann Nielsen and Jørgen Arendt Jensen

Center for Fast Ultrasound Imaging,
Biomedical Engineering group, Department of Electrical Engineering, Bldg. 349,
Technical University of Denmark, DK-2800 Kgs. Lyngby, Denmark

To be published in Proceedings of IEEE International Ultrasonics Symposium, Chicago, Il., USA, 2014.

In-Vivo Synthetic Aperture and Plane Wave High Frame Rate Cardiac Imaging

Matthias Bo Stuart*, Jonas Jensen*, Andreas Hjelm Brandt*†,
Svetoslav Ivanov Nikolov‡, Michael Bachmann Nielsen† and Jørgen Arendt Jensen*
*Center for Fast Ultrasound Imaging, Department of Electrical Engineering, Technical Univeristy of Denmark
†Department of Radiology, Copenhagen University Hospital, Denmark
‡BK Medical, Herlev, Denmark

***Abstract*—A comparison of synthetic aperture imaging using spherical and plane waves with low number of emission events is presented. For both wave types, a 90 degree sector is insonified using 15 emission events giving a frame rate of 200 frames per second. Field II simulations of point targets show similar resolution of approximately one wavelength radially and one degree angularly for both wave types. The use of spherical waves is found to have higher signal strength and better cystic resolution than plane waves. Measurements on wires in water yield similar results to simulations with similar resolution between the two wave types but better cystic resolution for spherical waves. Measurements on tissue mimicking phantoms show that both wave types penetrate down to 11 cm. Intensity measurements show an $I_{spta.3}$ of 18.4 mW/cm^2 for spherical waves and 22.7 mW/cm^2 for plane waves. The derated MI is 0.43 for spherical and 0.70 for plane waves. All measures are well within FDA limits for cardiac imaging. *In-vivo* images of the heart of a healthy 28-year old volunteer are shown.**

I. Introduction

A challenge in diagnostic ultrasound is the imaging of rapidly moving organs such as the heart. The faster the movement is, the less time is available for acquiring the image, which translates to a requirement for completing the acquisition using fewer emissions. A low number of emissions rules out line-by-line imaging leading to techniques using wide areas of insonification and beamforming of multiple lines per emission. Examples of such techniques are synthetic aperture [1], [2] and plane wave imaging [3].

The image quality characterized by the full width at half maximum (FWHM) and cystic resolution also depends on the number of emissions, where more emissions give higher image quality. There is a trade-off between frame rate and image quality. The question is then which of these two methods yields the best image quality. A quantitative comparison of synthetic aperture and plane wave imaging for phased array applications at 200 frames per second is therefore conducted.

II. Methods

This section describes synthetic aperture and multi-angle plane wave imaging. For both methods, a high frame rate (200 fps) has been targeted with a 90 degree sector view.

A. Synthetic Aperture

In synthetic aperture (SA) imaging [1], [2], an array of virtual sources (VS) is synthesized. Each VS is considered a point source for a spherical wave with a directivity pattern that depends on the physical aperture used to form the VS and the coordinates of the VS. For each VS, the echos received by each element in the physical transducer array are sampled.

The principle of synthetic aperture imaging is shown in Fig. 1. For each VS, the entire insonified area is imaged using delay-and-sum beamforming. This produces one low-resolution image for each VS. These low-resolution images are summed coherently to form a high-resolution image [4]. The high-resolution images are envelope detected and logarithmically compressed for display.

In this work, the in-phase and quadrature (IQ) signals are found from each transducer element using the Hilbert transform. This enables pixel-based beamforming, where only the pixels to be displayed on the screen are beamformed.

Fifteen VSs are placed behind the transducer on an arc with radius 10 mm spanning an arc of $84°$ in the setup used here.

B. Plane Wave

In plane wave (PW) imaging, the transmit delay profile follows a straight line as a function of the element x-coordinate for linear and phased array transducers. The slope of the line controls the direction of the plane wave.

As for SA imaging, the entire insonified area is imaged for each plane wave producing one low-resolution image for each PW. These are summed coherently to form high-resolution

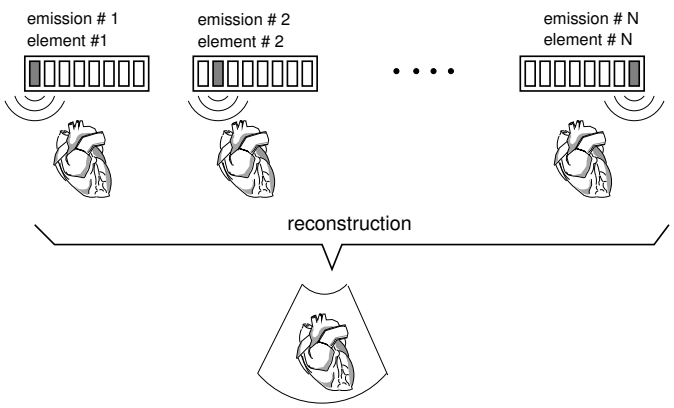

Fig. 1. The principle of synthetic aperture and multi-angle plane wave imaging. Figure from [4].

TABLE I
PARAMETERS USED IN THE SIMULATION

Parameter	Value
c	1480 m/s
f_0	3.5 MHz
Number of elements	128
Element pitch	$\lambda/2$
Element height	15 mm
Elevation focus	85 mm
Transmit apodization	Tukey, $\alpha = 0.1$
Radial scatterer positions	{25, 50, 75, 100, 125, 150} mm
Angular scatterer positions	{0°, 15°, 30°}

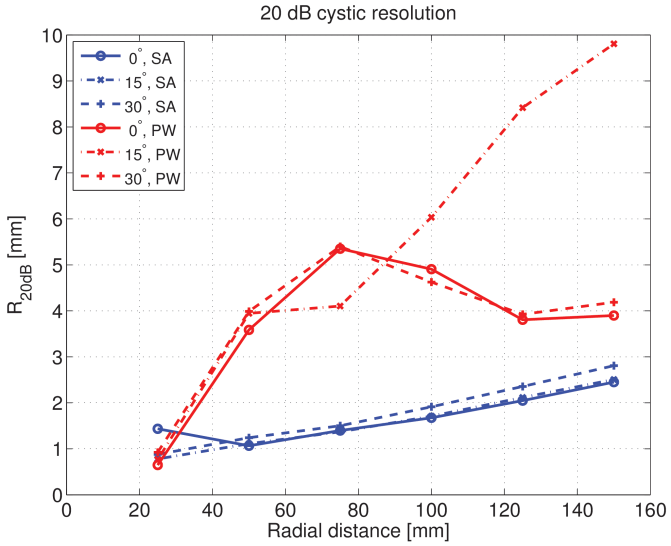

Fig. 2. 20 dB cystic resolution for the simulated PSFs.

images. The principle is exactly the same as for SA imaging with spherical waves as shown in Fig. 1. The only difference between the two is in the emission; the principle of processing the data is identical between the two wave types. Multi-angle plane wave imaging is often refered to as coherent compounding in the literature [3].

In this work, 15 plane waves with steering angles from $-42°$ to $42°$ are used. For each steering angle, the width of the plane wave, i.e., the extent of the insonified area, has been examined using simulations [5].

III. SIMULATIONS

Field II [6], [7] simulations are made of point targets with the simulation parameters shown in Table I. The scatterer positions are given in polar coordinates. For each emission, the received signals from all elements are stored for beamforming using an in-house beamformation toolbox [8].

The radial and angular FWHMs for the simulated point scatterers are approximately one wavelength and one degree respectively for all scatterer positions and both SA and PW.

Fig. 2 shows the 20 dB cystic resolution [9]. For SA the cystic resolution goes from 1 mm to 3 mm when the depth goes from 25 mm to 150 mm. The angle-dependence is minimal.

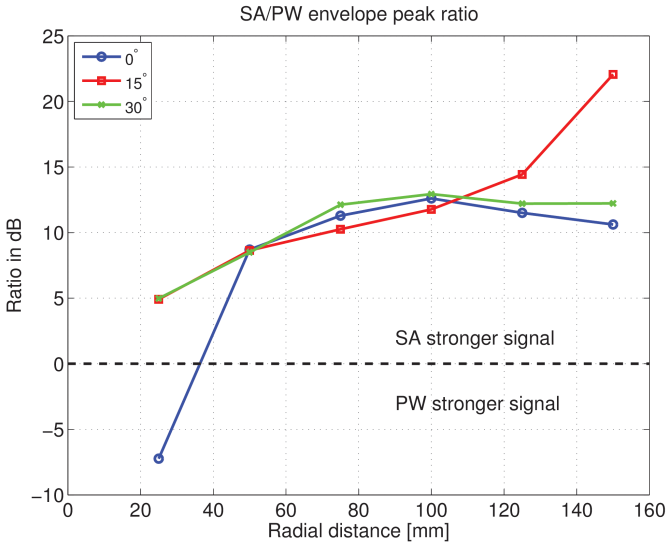

Fig. 3. Relative signal strength between synthetic aperture and plane wave imaging.

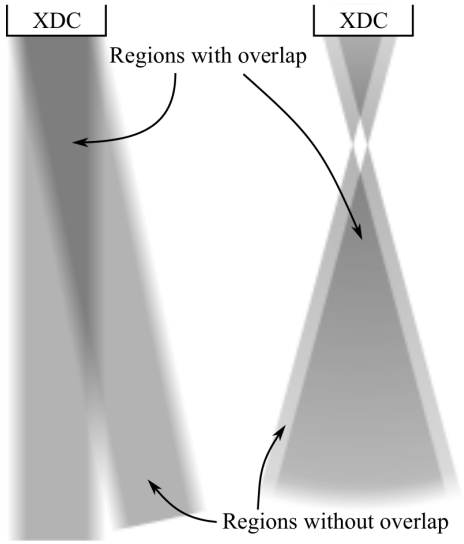

Fig. 4. Overlapping transmit fields for plane waves (left) and spherical waves (right).

For PW the cystic resolution mostly lies in the range from 4 mm to 5.5 mm. The exception is for $\theta = 15°$. This is due to the distribution of PW steering angles, where PWs are emitted at $\theta = 12°$ and at $\theta = 18°$, i.e., the energy in the direction $\theta = 15°$ is low resulting in poor image quality. This is illustrated in Fig. 4, which shows the insonified area of two plane and two spherical waves on the left and right, respectively. Close to the transducer, the two plane waves overlap fully. As the radial distance increases the overlapping area shrinks gradually, while at the same time, the parts of the waves that overlap are near the edge of the plane waves. As the transmit aperture is apodized to reduce side lobes, the energy at the edge is lower than at the center, as indicated by the lighter

TABLE II
METRICS FOR THE PSFS IN FIG. 5.

Metric	PW	SA
Angular FWHM	0.88°	0.95°
Lateral FWHM [mm]	1.30	1.41
Lateral FWHM λ	3.07	3.33
Axial FWHM [mm]	0.78	0.66
Axial FWHM λ	1.84	1.56
CTR 20 dB [mm]	5.31	2.12

coloring in the figure. Eventually an area is reached, which is insonified by neither plane wave, but this depth is below the imaged area for the setup used here. However, the point targets in the direction $\theta = 15°$ are in an area, where the overlap is close to the edges of the two plane waves. This contributes directly to the lower cystic resolution in this direction for plane wave imaging. For synthetic aperture, the energy is spread out over a larger area. This means that there are no areas, where it is only the edge of the spherical waves that overlap. This results in the more uniform cystic resolution across angles seen in Fig. 2.

This difference is also illustrated in Fig. 3, which shows the ratio of the peaks of the envelopes for the simulated scatterers. When using spherical waves, all emissions insonify all the scatterers, therefore the signal strength after summing of low-resolution images is in general 12 dB higher than for plane waves. In the direction $\theta = 15°$ the scatterers are located towards the edge of two plane waves resulting in 22 dB lower signal amplitude than that of synthetic aperture.

IV. PHANTOM MEASUREMENTS

A phased array identical to the one used in the simulation is used with the research scanner SARUS [10]. PSFs are measured on wires in water at $\theta = 0°$. The PSFs for a wire at $r = 85$ mm are shown in Fig. 5. The FWHM and 20 dB cystic resolution are reported in Table II. The two methods have similar resolution (FWHM), but the lower side lobe levels of SA translate to a better cystic resolution and a higher contrast. The lower side lobe levels come from the larger number of emissions insonifying the scatterer as illustrated in Fig. 4.

A tissue mimicking phantom (Model 571, Danish Phantom Design, Frederikssund, Denmark) with approximate speed-of-sound 1540 m/s and attenuation 0.5 dB/(cm·MHz) is used to measure the penetration depth. 100 frames were acquired using both plane and spherical waves. A single image line is beamformed along the z-axis for each frame. The mean of the 100 frames is taken to be the true signal, while the difference between a single frame and the mean is taken to be an instance of the system noise. The RMS voltage of both signal and noise are calculated along depth, and the SNR is calculated as the ratio between the two. This is shown in Fig. 6. The penetration depth is where the SNR equals 0, which is at approximately 11 cm for both SA and PW. Interestingly, the observations from Fig. 3 are not reflected in the measured SNR. This needs further investigation.

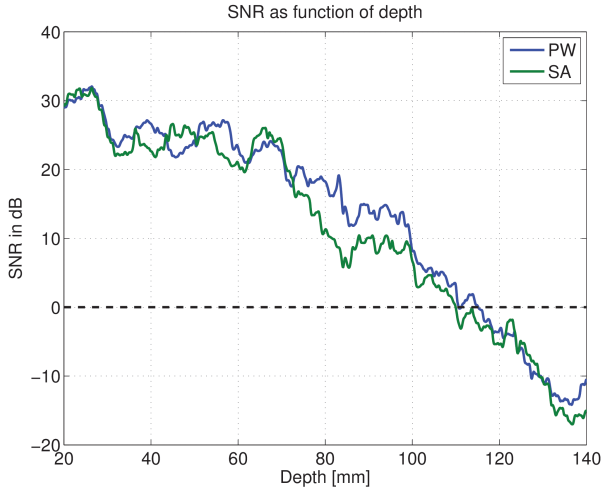

Fig. 6. The SNR as a function of depth.

V. *In-vivo* MEASUREMENT

To attain near-identical views spatially and temporally, the acquisition of PW and SA images is interleaved. Using a pulse repetition frequency of 3 kHz, this produces 100 fps of each method with a 5 ms separation between PW and SA images.

Mechanical index (MI) and spatial peak, temporal average intensity (Ispta) are measured using a hydrophone in a water tank (AIMS III, Onda Corporation, California) and an in-house intensity measurement framework [11]. An $I_{spta.3}$ of 18.4 mW/cm^2 is found for spherical waves and 22.7 mW/cm^2 for plane waves. The derated MI is 0.43 for spherical and 0.70 for plane waves. The respective FDA limits for cardiac imaging are 430 mW/cm^2 and 1.9.

For the *in-vivo* scan an echocardiography was performed. The echocardiography provides information about how the heart is structured and how each part of the heart is functioning. The medical doctor gets information about heart size, movement of valves and ventricular walls, and how blood flows through the different parts of the heart. A healthy 28-year old male volunteer was scanned in the preferred echocardiography scan positions (left lateral position and a supine position) to get a clear view of the left ventricular wall and valves.

Fig. 7 shows the beamformed images with 60 dB dynamic range. PW is shown on the left, SA is on the right. The figure shows the mitral valve and the outline of the left ventricle. The right ventricle can be glimpsed.

VI. CONCLUSION

This work compared the use of spherical and plane waves for phased array applications at 200 frames per second. Both wave types have similar resolution, but the use of spherical waves results in a better cystic resolution, which translates to higher contrast, and in a higher signal strength as more emissions insonify a given region. Both wave types have a penetration depth of approximately 11 cm in a homogeneous tissue mimicking phantom. *In-vivo* imaging (echocardiography) was

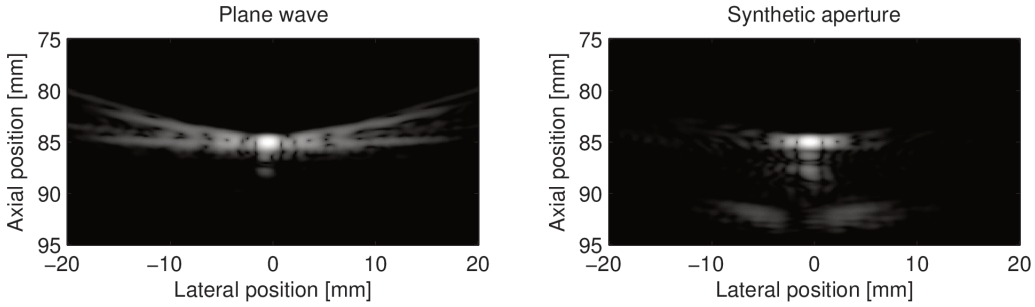

Fig. 5. PSFs for a wire in water at 85 mm depth. Both images are shown with 60 dB dynamic range and are individually normalized.

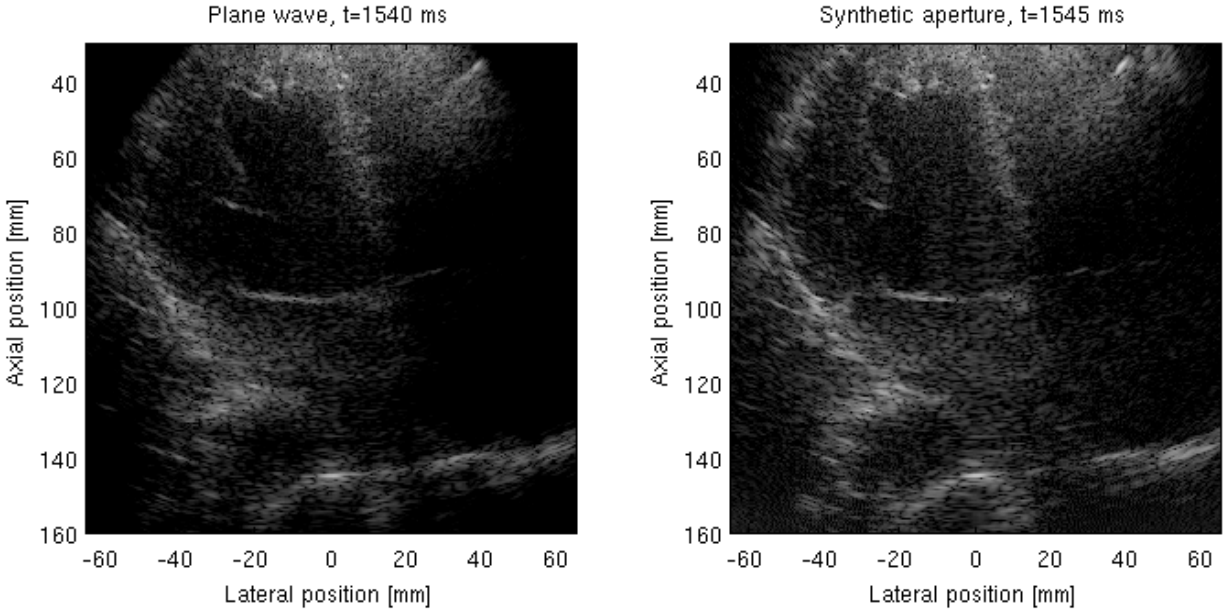

Fig. 7. In-vivo image of the mitral valve and left ventricle of a healthy 28-year old volunteer.

performed on a healthy 28-year old volunteer demonstrating the feasibility of high frame rate imaging using both synthetic aperture and plane wave imaging.

ACKNOWLEDGMENT

This work was supported by grant 82-2012-4 from the Danish National Advanced Technology Foundation and by BK Medical.

REFERENCES

[1] M. Soumekh, *Synthetic aperture radar. Signal processing with MATLAB algorithms*. New York: John Wiley & Sons, Inc., 1999.

[2] J. J. Flaherty, K. R. Erikson, and V. M. Lund, "Synthetic aperture ultrasound imaging systems," United States Patent, US 3,548,642, 1967, united States Patent, US 3,548,642, 1967, Published 22 Dec 1970.

[3] M. Tanter, J. Bercoff, L. Sandrin, and M. Fink, "Ultrafast compound imaging for 2-D motion vector estimation: application to transient elastography," *IEEE Trans. Ultrason., Ferroelec., Freq. Contr.*, vol. 49, pp. 1363–1374, 2002.

[4] S. I. Nikolov, "Synthetic Aperture Tissue and Flow Ultrasound Imaging," Ph.D. dissertation, Ørsted•DTU, Technical University of Denmark, 2800, Lyngby, Denmark, 2001.

[5] N. Oddershede and J. A. Jensen, "Effects influencing focusing in synthetic aperture vector flow imaging," *IEEE Trans. Ultrason., Ferroelec., Freq. Contr.*, vol. 54, no. 9, pp. 1811–1825, 2007.

[6] J. A. Jensen, "Field: A program for simulating ultrasound systems," *Med. Biol. Eng. Comp.*, vol. 10th Nordic-Baltic Conference on Biomedical Imaging, Vol. 4, Supplement 1, Part 1, pp. 351–353, 1996.

[7] J. A. Jensen and N. B. Svendsen, "Calculation of Pressure Fields from Arbitrarily Shaped, Apodized, and Excited Ultrasound Transducers," *IEEE Trans. Ultrason., Ferroelec., Freq. Contr.*, vol. 39, pp. 262–267, 1992.

[8] J. M. Hansen, M. C. Hemmsen, and J. A. Jensen, "An object-oriented multi-threaded software beamformation toolbox," in *Proc. SPIE Med. Imag.*, vol. 7968, March 2011, pp. 79 680Y 1–9. [Online]. Available: http://dx.doi.org/10.1117/12.878178

[9] K. Ranganathan and W. F. Walker, "Cystic resolution: A performance metric for ultrasound imaging systems," *IEEE Trans. Ultrason., Ferroelec., Freq. Contr.*, vol. 54, no. 4, pp. 782–792, 2007.

[10] J. A. Jensen, H. Holten-Lund, R. T. Nilsson, M. Hansen, U. D. Larsen, R. P. Domsten, B. G. Tomov, M. B. Stuart, S. I. Nikolov, M. J. Pihl, Y. Du, J. H. Rasmussen, and M. F. Rasmussen, "SARUS: A synthetic aperture real-time ultrasound system," *IEEE Trans. Ultrason., Ferroelec., Freq. Contr.*, vol. 60, no. 9, pp. 1838–1852, 2013.

[11] J. A. Jensen, M. F. Rasmussen, M. B. Stuart, and B. G. Tomov, "Rapid measurements of intensities for safety assessment of advanced imaging sequences," in *Proc. SPIE Med. Imag.*, 2014, p. In Press.